INTERNATIONAL JOURNAL FOR NUMERICAL METHODS IN FLUIDS, VOL. 16, 813–825 (1993)

MODELLING LARGE-BUBBLE FORMATION AT SUBMERGED ORIFICES

J. D. BUGG

Department of Mechanical Engineering, The University of Saskatchewan, Saskatoon, Saskatchewan, Canada, S7N 0W0

AND

R. D. ROWE

Department of Mechanical Engineering, The University of Calgary, 2500 University Drive NW, Calgary, Alberta, Canada, T2N 1N4

SUMMARY

The formation of large gas bubbles at submerged orifices is investigated numerically with a two-dimensional, transient, finite difference model using a volume fraction specification to track the movement of the gas–liquid interface. Experimentally observed features of large-bubble formation such as the initial toroidal shape of the bubbles and the penetration of liquid down the pipe centreline are well predicted by the model. The expected oscillatory nature of growth is also observed. The bubble departure volume corresponds to experiments and to the model of Davidson and Schuler. At present the simulations do not extend far enough to investigate multiple-bubble ejection and important bubble-to-bubble interactions during growth and after departure.

KEY WORDS Bubble formation Bubble growth Bubbling regimes Free boundaries Interface advection

INTRODUCTION

Bubble formation at submerged orifices has been investigated by many people. However, the literature is dominated by work with small orifices (<2 cm). A good account of bubbling behaviour from small orifices is provided by McCann and Prince.[1] They classified three general bubbling regimes: static, dynamic and turbulent. Static bubbling is governed purely by buoyancy and surface tension and a simple static balance of these forces predicts the bubble departure volume. As the gas flow rate and orifice diameter increase, inertial forces become important and the dynamic regime is entered. The resulting growth and immediate post-departure behaviour become much more complicated. The bubble generation rate becomes large enough that there is significant bubble-to-bubble interaction and bubble releases can no longer be treated as simple independent events. To distinguish between different types of interaction, McCann and Prince[1] further subdivide the dynamic regime into single and double bubbling, single and double pairing, and delayed release. Upon further flow rate increases, the turbulent regime is entered where the flow becomes more like a jet and no distinct periodic bubble formation occurs.

The literature concerning bubble formation from large orifices is much more sparse. Large bubbles are of interest in applications such as underwater detonations,[2,3] fluidized beds,[4] nuclear reactor accident analysis[5,6] and the blow-out of undersea oilwells.[7,8] The fundamental difference

0271–2091/93/090813–13$11.50

Received September 1992
Revised November 1992

between large and small bubbles is the reduced magnitude of the stabilizing surface tension forces. For bubbles not attached to a gas supply, increasing size results in shape changes for a steadily rising bubble which progress from spherical (for small bubbles) through oblate spheroids and finally to spherical caps. A good discussion of this progression is provided by Harper.[9] The behaviour and maximum size of spherical caps are discussed by Davies and Taylor[10] and Batchelor.[11] A measure of what constitutes a 'small' bubble is usually the Eotvos number (ratio of buoyancy to surface tension forces) as discussed in Reference 12. Large spherical air bubbles in water do not exist unless they are growing. Once growth stops, they quickly shatter into smaller bubbles. The large-bubble literature, then, is concerned with bubbles growing at orifices[5-8] or by the action of expanding gases.[2, 3]

Chen and Dhir[6] considered the dynamics of a boiling water reactor pressure suppression pool when gas was injected into it through a large downward-facing pipe. Pipe diameters investigated were from 9 to 95 mm with air flow rates of 3–80 $l\,s^{-1}$. A large part of their work was concerned with the vent-clearing process and few details of bubble volume or shape upon departure were reported. Topham[7] injected nitrogen through orifices ranging from 6·4 to 145 mm at flow rates up to 32 $l\,s^{-1}$. Rounded bubbles growing from the orifice, releasing and quickly bursting into smaller fragments were observed. As the flow rate was increased, the bubbles become flattened horizontally and breakaway was again characterized by violent bursting. No data concerning departure volume or bubble interaction were reported.

The numerical investigation in this paper parallels an experimental investigation[8] of large-bubble formation in an apparatus shown schematically in Figure 1. The two key parameters varied in this investigation were the pipe diameter ($25{\cdot}4 \leqslant D \leqslant 101{\cdot}6$ mm) and the gas flow rate ($5 \leqslant Q \leqslant 50\ l\,s^{-1}$). Bubbles were produced in a 1·22 m square by 1·22 m high cast acrylic water tank. Air flow to the apparatus was measured by a circular arc, critical venturi meter. After the flow meter, the air entered a plenum chamber mounted under the centre of the tank. Pipes of various sizes were mounted on the plenum chamber so that they protruded through the centre of the tank floor. Bubble growth at the pipe exit was recorded with a 16 mm rotating prism, high-speed movie camera (Hycam). Timing marks were provided by an internal timing light

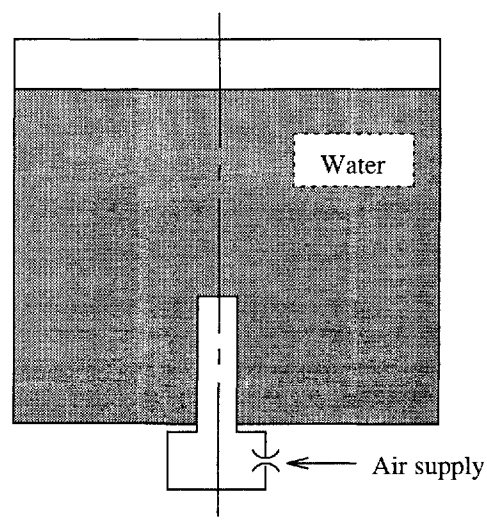

Figure 1. Schematic diagram of apparatus to produce large bubbles

driver running at 100 Hz. Quantitative information was extracted by projecting the high-speed films onto a digitizing pad and tracing the outline of each bubble. The bubble volume was estimated by revolving the bubble profile around the pipe axis by 180°.

The experiments revealed several regimes of bubble behaviour over the conditions tested. At low flow rates and large pipe diameters there is such significant penetration of liquid into the pipe (back-flooding) that the pipe exit is not a site for bubble formation. This means that the static bubbling regime described for small orifices by McCann and Prince[1] does not exist for large orifices where a stable static interface as large as the pipe diameter cannot be maintained. As the flow rate is increased, a transition region is entered where large irregular bubbles are intermittently formed at the pipe exit. Upon further flow rate increase the double-bubbling regime is entered. No distinct single-bubbling or single-pairing regimes (as described by McCann and Prince[1]) were observed for large orifices. The first bubble in a doublet grows and departs with little influence from bubbles which have been released previously. The second bubble is elongated along the pipe axis and departs prematurely under the strong influence of the flow field induced by the movement and distortion of the first bubble. It is swept very quickly upwards into the first bubble and the two form a very unstable large bubble which quickly shatters. The cycle then repeats itself. After another transition region in which 'double-bubbling-type' bubble-to-bubble interaction takes place between more than two consecutive bubbles, the final regime of continuous interaction is entered. Here all bubbles are heavily influenced by the previous bubbles released. This is the turbulent regime described by McCann and Prince.[1]

A key result of the experiments was that when Q and D are the quantities varied, the regime boundaries lie on lines of constant Froude number ($F = Q/\sqrt{(gD^5)}$). Note that McCann and Prince[1] also identified the capacitance of the chamber supplying the orifice as a governing factor in determining the bubbling regime, but this quantity was not varied significantly in Reference 8.

NUMERICAL MODEL

The numerical procedure is discussed in detail in Reference 13 and in brief in Reference 14. It uses an approach similar to the SOLA-VOF technique[15] and solves the two-dimensional, transient form of the Navier–Stokes equations using a volume-tracking technique to specify the position of the gas–liquid interface. This interface is advected using the donor–acceptor algorithm of Hirt and Nichols.[16] Because the interface advection algorithm contains an inherent restriction that the Courant number be less than unity, an explicit scheme is used to advance the underlying flow field solution in time.

Model geometry

The application of the numerical model to the experiments will now be described. A cylindrical co-ordinate system (r, z) assuming axisymmetry about the centreline of the pipe is used and extends to a radius of 0·688 m. The boundaries of the air delivery pipe are modelled by blocking control volumes at the appropriate radius. All solid boundaries are modelled with zero-penetration, free slip boundary conditions. Since the near-wall grid is too coarse to resolve the boundary layer, a free slip boundary condition provides a more accurate representation of the near-wall velocity profile than does the no-slip condition. A discussion of this point can be found in Reference 17. The depth of liquid is matched to the experiments and is equal to 1·067 m for all runs. The initial condition is a quiescent liquid with a horizontal gas–liquid interface at the pipe exit (as shown in Figure 1).

In order to save storage and increase speed, a non-uniform grid is used. The r-direction grid is designed to be used for any of the four pipe diameters (25·4, 50·8, 76·2 and 101·6 mm) by specifying a uniform grid region extending from $r=0$ to 0·010 16 m, twice the radius of the largest pipe. Within this region $\delta r = 4{\cdot}2\overline{3}$ mm, so that two control volumes must be blocked to equal the actual pipe wall thickness. This δr also ensures that all four possible pipe radii fall on control volume boundaries. From $r=0{\cdot}01016$ to 0·688 m δr increases linearly by 0·075 15 mm each control volume to give a total of 105 control volumes in the r-direction.

The z-direction grid contains 190 control volumes. A uniform region with $\delta z = 4.2\overline{3}$ mm extends 24 control volumes, or twice the radius of the largest pipe, upwards from the exit of the pipe. From this concentrated region the control volumes increase in size linearly with z towards the top and bottom of the solution domain. The full domain contains 19 950 control volumes. A typical run in this paper advances the solution to $t=0{\cdot}2$ s in 2000 time steps and requires approximately 40 min CPU time on a two-pipe Cyber 205.

Gas pressure model

The gas volume in the pipe and attached bubble is calculated from the volume fraction of liquid field, f. Changes in this volume result directly from changes in the f-field calculated by the interface advection algorithm in response to the calculated velocity field. The gas pressure model adds 3·64 l to this volume to account for the chamber supplying the pipe. The gas pressure is adjusted each time step on the basis of the influx of a constant mass flow rate into this total volume and an isentropic expansion/compression of the gas volume.

RESULTS AND DISCUSSION

The model was run over a variety of conditions in the experimental run matrix ($25{\cdot}4 \leqslant D \leqslant 101{\cdot}6$ mm, $5 \leqslant Q \leqslant 50\,\mathrm{l\,s^{-1}}$). Several features of bubble growth identified in the experiments will now be compared with the numerical results. The first is the penetration of liquid down the pipe centreline, followed by a discussion of the toroidal bubble shape during the initial growth stage. Next, the oscillatory nature of bubble growth is considered, as is the behaviour of the model during necking and departure. Finally, the model's ability to predict the bubble volume in the double-bubbling regime will be addressed.

Centreline penetration

At low flow rates and large pipe diameters there is a strong tendency for liquid to penetrate down the centreline of the pipe. This is evident in the experiments[13] and constitutes a major source of back-flooding. The numerical results clearly show this tendency. A measure of centreline penetration is the vertical movement of the gas–liquid interface on the pipe centreline. All computational runs show some initial upward movement at the centreline. At low flow rates and large pipe diameters this movement reverses and causes significant penetration of liquid into the pipe. However, for higher flow rates and smaller pipe diameters no such reversal occurs. Two simulations will now be presented to illustrate these effects. Figures 2, 3 and 7 are not the entire solution domain but rather a $0{\cdot}5 \times 0{\cdot}5\ \mathrm{m^2}$ region near the pipe exit. The time of each frame is given in both dimensional and non-dimensional forms ($T = t\sqrt{(g/D)}$).

Figure 2 is a prediction of $42{\cdot}5\ \mathrm{l\,s^{-1}}$ flow through a 76·2 mm pipe. Although the interface on the pipe centreline initially moves upwards, a very significant tongue of liquid penetrates down the centreline of the pipe. In contrast, Figure 3 illustrates a $17\ \mathrm{l\,s^{-1}}$ flow through a 25·4 mm diameter

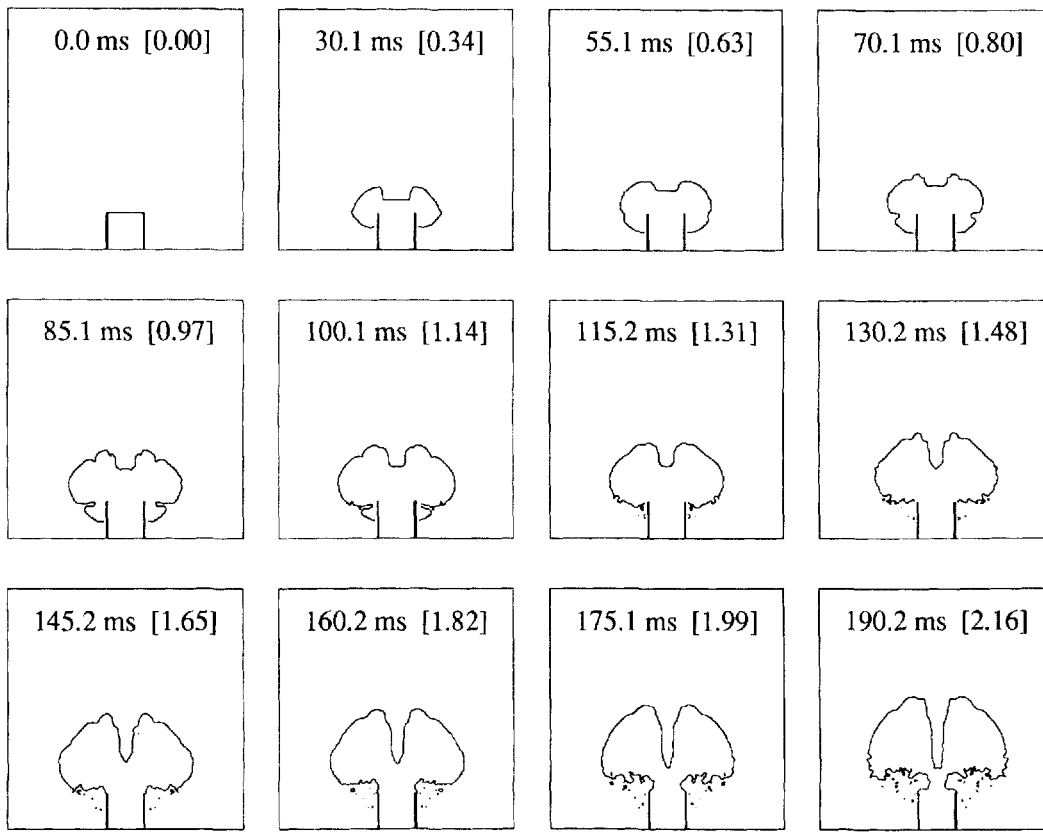

Figure 2. Simulated large-bubble growth for $D = 76{\cdot}2$ mm, $Q = 42{\cdot}51\,s^{-1}$, $F = 85$

pipe. Here the gas–liquid interface at the centreline moves strongly upwards throughout the entire simulation, preventing the formation of a penetrating liquid tongue.

Figure 4 plots the vertical displacement of the gas–liquid interface on the centreline versus time for a number of simulations. The Froude number is shown at the end of each curve plotted. This figure illustrates the initial upward motion which occurs under all conditions investigated. At low Froude numbers this upward motion reverses and the vertical position begins to fall. However, as the Froude number is increased, a critical value is reached past which no reversal takes place and the top of the bubble moves upwards throughout the entire time the bubble is attached to the pipe. It is estimated that this critical Froude number is approximately 10.

Another quantity of interest is the curvature of the surface at the pipe centreline. In Figure 2 the penetrating liquid on the centreline is concave towards the liquid side of the interface. This is also true during the early stages of Figure 3. However, in the latter case bubble growth is vigorous enough that the curvature changes to concave towards the gas side of the interface. This reversal of curvature is not a necessary condition for a reversal in the direction of movement on the centreline. A range of conditions exists where the curvature continues to be concave towards the liquid but the interface continues to move upwards. The critical Froude number for the curvature to become concave towards the gas is about 50.

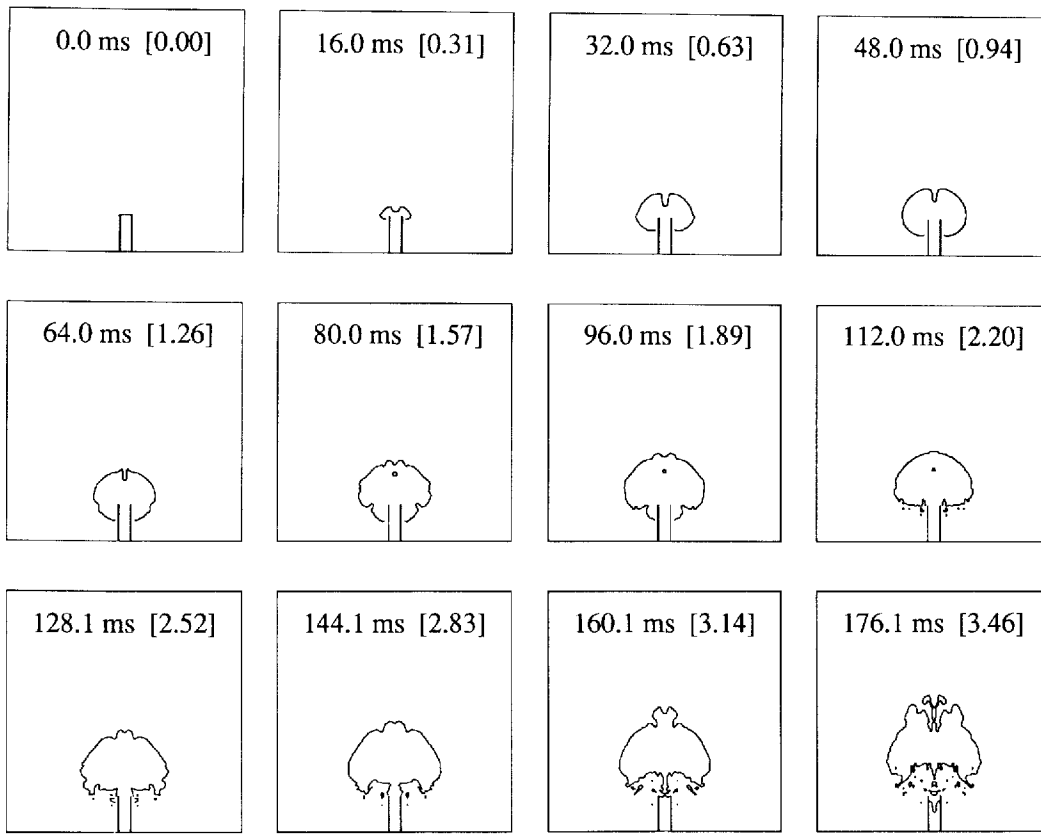

Figure 3. Simulated large-bubble growth for $D = 25{\cdot}4$ mm, $Q = 17{\cdot}0\,\mathrm{l\,s^{-1}}$, $F = 53$

The reversal of curvature is shown in Figure 4 as a sudden jump in the vertical position of the interface. The reason for this discontinuity can be seen in Figure 3. The curvature reversal process involves the necking of the penetrating tongue of liquid and subsequent shedding of a droplet of liquid inside the bubble. At the instant contact is made, the vertical position on the centreline suddenly increases.

The other back-flooding mechanism identified in the experiments was the necking and departure process. Because of the incomplete prediction of the departure process, it is difficult to determine the back-flooding boundary due to this mechanism. Some predictions show what appears to be quite substantial back-flooding by this mechanism. However, this occurs because the code is late in identifying departure. If proper departure had occurred, the pressure in the pipe would rise more quickly, reducing the tendency for liquid to enter the pipe.

Initial toroidal bubble formation

As stated previously, the initial movement of the gas–liquid interface on the pipe centreline is always upwards. Another feature that is ubiquitous over the range of conditions tested is that the bubble always begins its growth as a toroid. This means that although the movement is upwards at the pipe centreline, bubble growth is faster near the edge of the pipe. This can be clearly seen in Figures 2 and 3 and was also very apparent in the experimental results.[13]

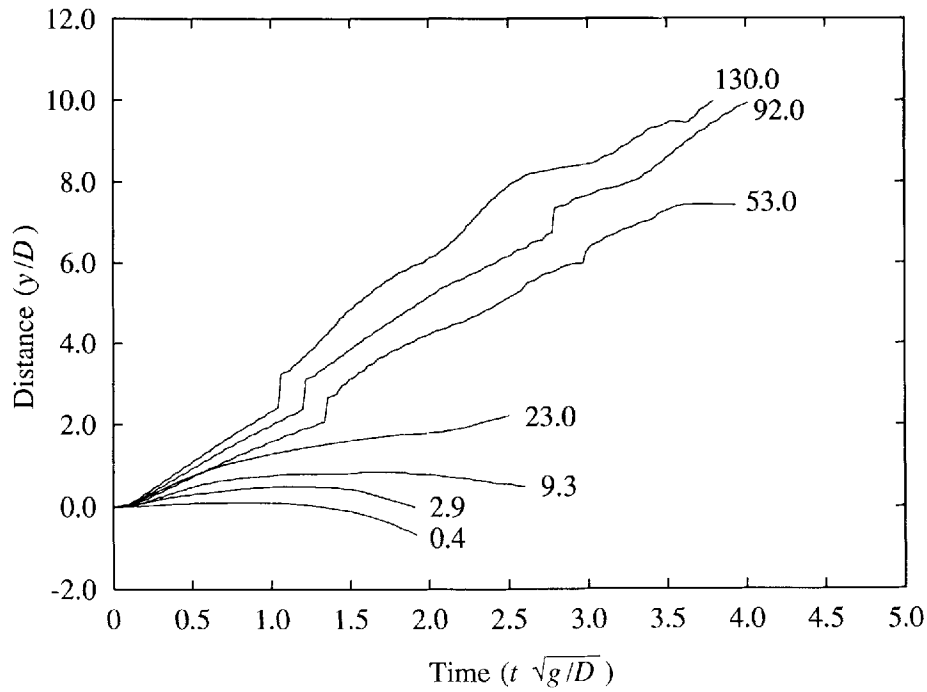

Figure 4. Vertical movement of interface on centreline for various Froude numbers

At the beginning of the simulations, pressure equilibrium exists across the gas–liquid interface. As the solution begins, an overpressure builds in the gas owing to the gas flow into the pipe. Growth at the pipe edge occurs in both the r- and z-directions, while at the pipe centreline the symmetry constrains growth to the z-direction only. An illustration of the initial behaviour is given by the streamline plots in Figure 5 for 43·6 $1\,s^{-1}$ from a 50·8 mm pipe. The concentration of streamlines near the pipe edge indicates the higher velocity there compared with the pipe centreline. In later frames this preferential growth has resulted in the formation of a toroidal bubble.

Oscillatory bubble growth

When a bubble begins growth in a quiescent fluid, the pressure builds in the pipe to a value which exceeds that required to maintain a constant growth rate. The liquid accelerates away from the bubble until its momentum overexpands the bubble, causing the pressure to drop below that required for a constant growth rate. The result is oscillations in bubble pressure and volume. This phenomenon is discussed by Chen and Dhir[6] in connection with the vent-clearing process and can be predicted by a simultaneous solution of the extended Rayleigh equation and a gas pressure model for constant mass flow into the bubble. The model results clearly show the oscillatory bubble growth expected.

Figure 6 shows that in general the bubble growth rate is properly predicted by the numerical model in the current study. However, the experimental oscillation amplitude is much smaller. Recall that the initial condition for the numerical results is a quiescent liquid with a horizontal gas–liquid interface at the pipe exit. The experimental work is based on observations made well

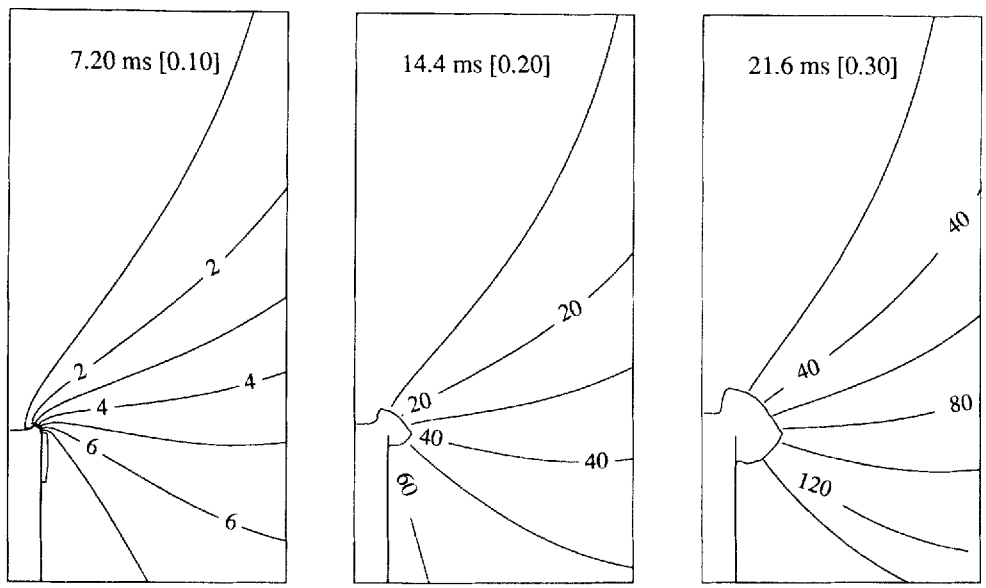

Figure 5. Stoke's streamfunction ($\Psi \times 10^4$ m^3 s^{-1}) during the early stages of bubble growth for $D = 50{\cdot}8$ mm, $Q = 43{\cdot}61\,\mathrm{s}^{-1}$, $F = 24$

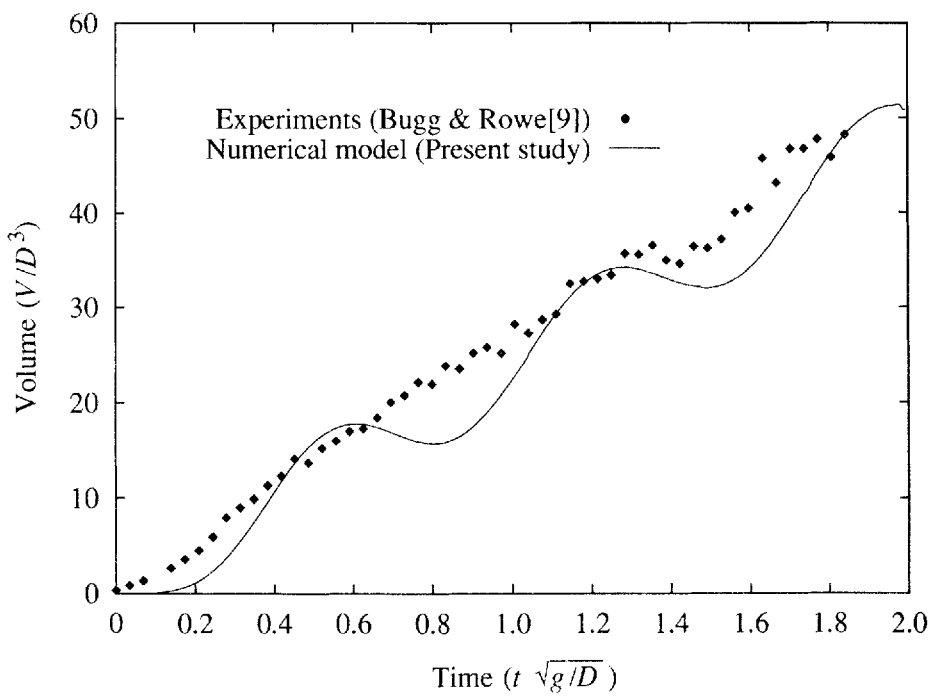

Figure 6. Predicted and experimental bubble growth for $D = 50{\cdot}8$ mm, $Q = 43{\cdot}61\,\mathrm{s}^{-1}$

after start-up, when a quasi-steady, periodic state has been reached. This means that some overall circulation has been established in the tank and the local influence of the previous bubble released is present. The resulting upward liquid velocity near the pipe exit would assist the bubble growth process and reduce the gas overpressure required to overcome the liquid's inertia near the pipe exit, thus accounting for the reduced oscillation amplitude observed experimentally.

Departure

Currently, the simulations progress only to the point where the bubble departs. The collapse of the model can be traced to the inability of the interface advection algorithm to maintain a distinct interface under the combined complications of oscillatory bubble growth, necking and departure at the pipe exit and the strong circulation induced by departure and subsequent deformation.

Consider Figure 3, where 17 l s^{-1} is being ejected from a 25·4 mm pipe. During the intermediate stages of bubble growth ($0{\cdot}75 < T < 1{\cdot}2$) the bubble is essentially centred on the pipe exit. As the bubble grows larger, the buoyancy force becomes quite significant and the bubble begins to lift. At $T \approx 2$ it rises so that its lower surface is at the pipe exit. As it rises beyond this point, the necking process begins ($T = 2{\cdot}8$). As the bubble rises away from the pipe exit, the region between the pipe exit and the lower surface of the bubble becomes dominated by partially full control volumes. The primary result is that no distinct surface can be defined. Another important result is

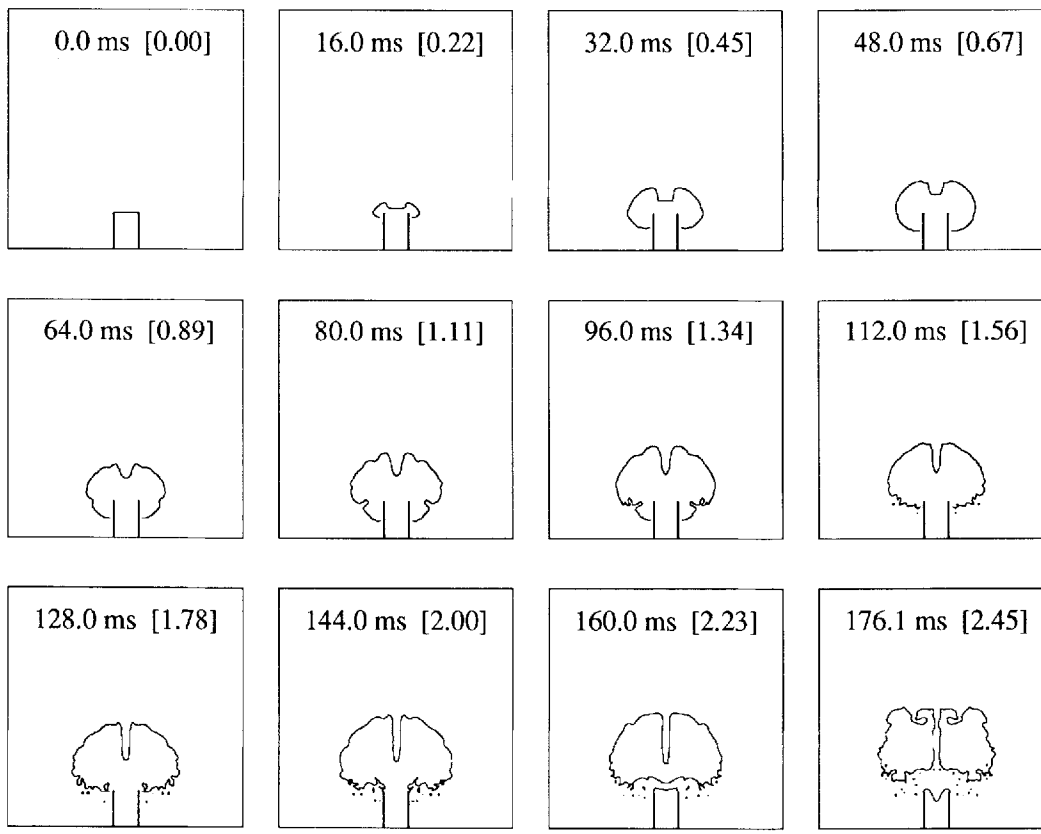

Figure 7. Simulated large-bubble growth for $D = 50{\cdot}8$ mm, $Q = 29{\cdot}7$ l s^{-1}, $F = 19$

that a continuous path of partially full control volumes connects the large bubble just produced to the gas in the pipe. As a consequence, the bubble continues to grow as though it were attached for some time after it appears to have departed.

Departure volume

Since the simulations survive only up to the departure of the first bubble, a full simulation of a double-bubbling cycle has not been achieved. However, since the critical feature of the first bubble is that it is influenced very little by bubbles released before it, the simulations should display much the same behaviour as the first bubble in a doublet. On this basis a comparison of the departure volume predicted by the simulations will be made with experimental results in the double-bubbling regime.

A simulation in the double-bubbling regime is given in Figure 7, where a flow rate of 29·7 l s^{-1} from a 50·8 mm pipe is illustrated. The departure time for the model results is obtained by inspecting bubble profile histories such as given in Figure 7 and determining when the necking process is complete. This simulation indicates that departure occurs at 160 ms when the volume is 4.6 l. A departure volume of about 5 l was observed for these experimental conditions.

Figure 8 shows the departure volume for all simulations in the double-bubbling regime compared with the experimental departure volumes observed. The model appears to predict the volume of the first bubble of a doublet very effectively. It is interesting to note that the very simple relationship developed by Davidson and Schuler[18] correlates quite well with these results. It is

$$V = 1{\cdot}378 Q^{1{\cdot}2}/g^{0{\cdot}6} \tag{1}$$

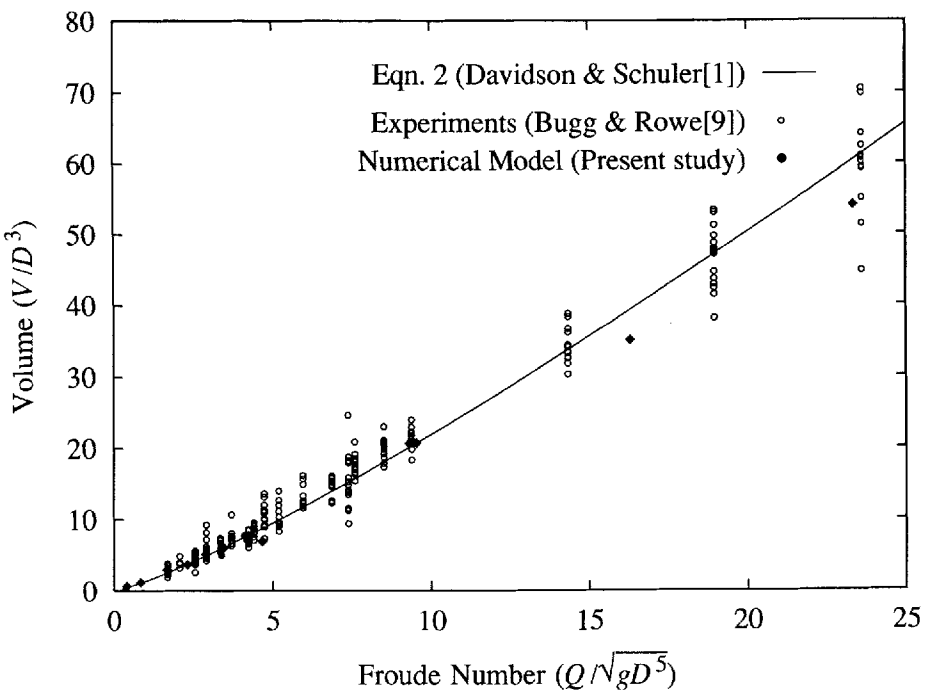

Figure 8. Departure volume of first member of a doublet as a function of Froude number

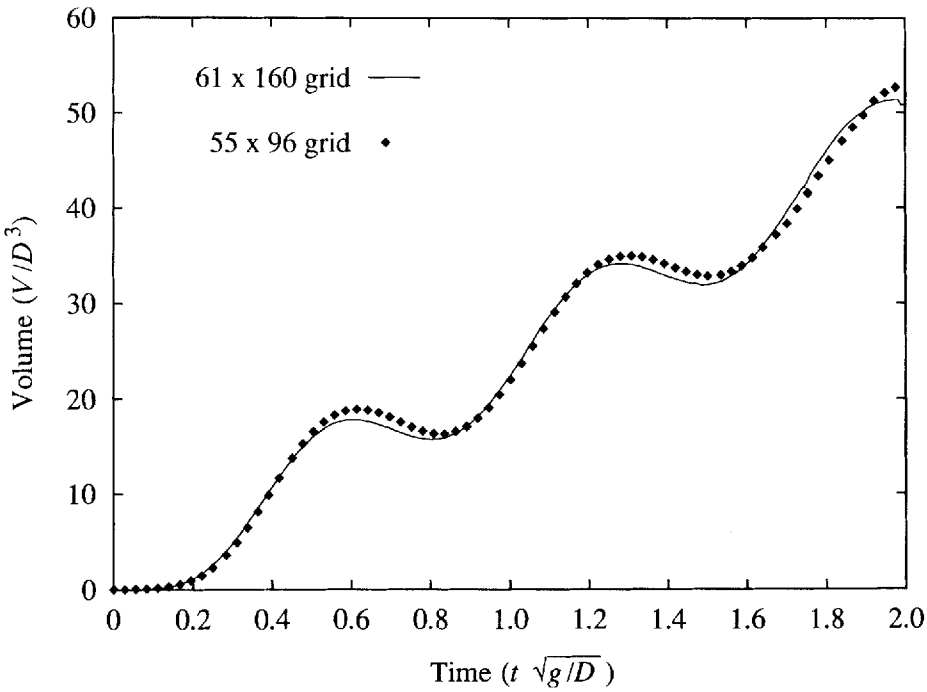

Figure 9. Grid independence test for $D = 50{\cdot}8$ mm, $Q = 43{\cdot}61\,s^{-1}$, $F = 24$

and can be written as follows in dimensionless form:

$$V/D^3 = 1{\cdot}378\ F^{1{\cdot}2} \tag{2}$$

This equation was developed by balancing the buoyancy force with the upward acceleration of the surrounding fluid for a growing spherical bubble. Departure was defined as the point when the growing sphere rises by an amount equal to its radius. This is similar to the visual criterion used to establish the departure volume for the current numerical model as discussed earlier.

Grid independence

Confidence of grid-independent results is gained from preliminary runs that were done with a 55×96 rather than a 105×190 grid. Up to the time of bubble departure these runs are very similar. A representative result is given in Figure 9, which shows the volume history for each grid resolution. After departure, when the interface becomes highly distorted, the grid resolution has a marked effect on interface advection. This effect occurs before grid dependences in the velocity field calculation become apparent.

CONCLUSIONS

It has been demonstrated that it is possible to numerically model several important features of large-bubble growth at submerged orifices. The initial growth as a toroid and the penetration of liquid down the centreline are modelled very well. The bubble volume calculation has been demonstrated to be quite realistic, in accordance with experiments[8] and the model of Davidson

and Schuler.[18] The problems of effectively modelling departure and post-departure behaviour relate to the inability of the interface advection algorithm to maintain a distinct gas–liquid interface. Much work is still required in this area before solutions can be advanced significantly further in time and begin to show the type of bubble-to-bubble interaction which dominates the region above the pipe exit.

ACKNOWLEDGEMENTS

This work has been supported by a contract from the Environmental Emergencies Technology Division of Environment Canada and an operating grant from the Canadian Natural Sciences and Engineering Research Council.

APPENDIX: NOMENCLATURE

D	pipe diameter
E	Eotvos number ($gD^2\rho/\sigma$)
F	Froude number ($Q/\sqrt{(gD^5)}$)
g	acceleration due to gravity
Q	volume flow rate
t	time
T	dimensionless time ($t\sqrt{(g/D)}$)
V	volume

Greek letters

δr	grid spacing in r-direction
δz	grid spacing in z-direction
ρ	liquid density
σ	surface tension

REFERENCES

1. D. J. McCann and R. G. H. Prince, 'Regimes of bubbling at a submerged orifice', *Chem. Eng. Sci.*, **26,** 1505–1512 (1971).
2. Lord Rayleigh, 'On the pressure developed in a liquid during the collapse of a spherical cavity', *Phil. Mag., Ser. 6,* **34,** 94–98 (1917).
3. S. A. Wilkerson, 'Boundary integral techniques for explosion bubble collapse', *Energy Sources Technology Conf. and Exhibition,* American Society of Mechanical Engineers, New York, Paper #89-OCN-2, Houston, TX, January 1989.
4. R. Clift, J. R. Grace and M. E. Weber, 'Stability of bubbles in fluidized beds', *Ind. Chem. Eng. Fund.*, **13,** 45–51 (1974).
5. W. J. Marble, T. L. Wong, F. J. Moody and D. A. Hankins, 'Retention of fission products by BWR suppression pools during severe reactor accidents', *Int. Thermal Nuclear Reactor Safety Conf.*, American Nuclear Society, Chicago, IL, 1982.
6. C. L. Chen and V. K. Dhir, 'Hydrodynamics of a bubble formed at vent pipe exit', *Int. J. Multiphase Flow,* **8,** 147–163 (1982).
7. D. R. Topham, 'Hydrodynamics of an oilwell blowout', *Beaufort Sea Technical Report 33,* Institute of Ocean Sciences, Sydney, BC, 1975.
8. J. D. Bugg and R. D. Rowe, 'Bubbling regimes at the wellhead of a subsea oilwell blowout', *Proc. 11th Int. Conf. on Offshore Mechanics and Arctic Engineering,* Calgary, June 1992, ASME, New York, 1992, pp. 571–576.
9. J. F. Harper, 'The motion of bubbles and drops through liquids', *Adv. Appl. Mech.*, **12,** 59–129 (1972).
10. R. M. Davies and G. I. Taylor, 'The mechanics of large bubbles rising through extended liquids and through liquids in tubes', *Proc. R. Soc. A.*, **200,** 375–390 (1950).
11. G. K. Batchelor, 'The stability of a large gas bubble rising through liquid', *J. Fluid. Mech.*, **184,** 399–422 (1987).
12. R. Clift, J. R. Grace and M. E. Weber, *Bubbles, Drops and Particles,* Academic, New York, 1978.

13. J. D. Bugg, 'An investigation of large bubble dynamics', *Ph.D. Thesis*, University of Calgary, 1991.
14. J. D. Bugg and R. D. Rowe, 'Modelling the initial motion of large cylindrical and spherical bubbles', *Int. j. numer. methods fluids*, **13,** 109–129 (1991).
15. B. D. Nichols, C. W. Hirt and R. S. Hotchkiss, 'SOLA-VOF: a solution algorithm for transient fluid flow with multiple free boundaries', *Technical Report LA-8355*, Los Alamos National Laboratories, 1980.
16. C. W. Hirt and B. D. Nichols, 'Volume of fluid (VOF) method for the dynamics of free boundaries', *J. Comput. Phys.*, **39,** 201–225 (1981).
17. C. W. Hirt, 'Introduction to numerical solution of industrial flows', *Lecture Series 1986-07*, von Karman Institute for Fluid Dynamics, 1986.
18. J. F. Davidson and B. O. G. Schuler, 'Bubble formation at an orifice in an inviscid liquid', *Trans. Inst. Chem. Eng.*, **38,** 335–342 (1960).